CHEMISTRY OF MATERIALS
Cite This: Chem. Mater. 2019, 31, 73−82
Article
pubs.acs.org/cm

Designing Conjugated Polymers for Molecular Doping: The Roles of Crystallinity, Swelling, and Conductivity in Sequentially-Doped Selenophene-Based Copolymers

D. Tyler Scholes,[†] Patrick Y. Yee,[†] George R. McKeown,[‡] Sheng Li,[‡] Hyeyeon Kang,[†] Jeffrey R. Lindemuth,[¶] Xun Xia,[†] Sophia C. King,[†] Dwight S. Seferos,[‡] Sarah H. Tolbert,*[,†] and Benjamin J. Schwartz*[,†]

[†]Department of Chemistry and Biochemistry, University of California, Los Angeles, Los Angeles, California 90095-1569, United States

[‡]Department of Chemistry, University of Toronto, Toronto, Ontario M5S 3H6, Canada

[¶]Lake Shore Cryotronics, Westerville, Ohio 43082, United States

Supporting Information

ABSTRACT: Although chemical doping is widely used to tune the optical and electrical properties of semiconducting polymers, it is not clear how the degree of doping and the electrical properties of the doped materials vary with the bandgap, valence band level, and crystallinity of the polymer. We addressed these questions utilizing a series of statistical copolymers of poly(3-hexylthiophene) (P3HT) and poly(3-heptylselenophene) (P37S) with controlled gradients in bandgap, valence band position, and variable crystallinity. We doped the copolymers in our series with 2,3,5,6-tetrafluoro-7,7,8,8-tetracyanoquinodimethane (F_4TCNQ) using solution sequential processing. We then examined the structures of the films using grazing incidence wide-angle X-ray scattering, differential scanning calorimetry, and ellipsometric porosimetry, and the electrical properties of the films via the AC Hall effect. We found that the ability of a particular copolymer to be doped is largely determined by the offset of the polymer's valence band energy level relative to the LUMO of F_4TCNQ. The ability of the carriers created by doping to be highly mobile and thus contribute to the electrical conductivity, however, is controlled by how well the polymer can incorporate the dopant into its crystalline structure, which is in turn influenced by how well it can be swelled by the solvent used for dopant incorporation. The interplay of these effects varies in a nonmonotonic way across our thiophene:selenophene copolymer series. The position and shape of the polaron absorption spectrum correlate well with the polymer crystallinity and carrier mobility, but the polaron absorption amplitude does not reflect the number of mobile carriers, precluding the use of optical spectroscopy to accurately estimate the mobile carrier concentration. Overall, we found that the degree of crystallinity of the doped films is what best correlates with conductivity, suggesting that only carriers in crystalline regions of the film, where the dopant counterions and polarons are forced apart by molecular packing constraints, produce highly mobile carriers. With this understanding, we are able to achieve conductivities in this class of materials exceeding 20 S/cm.

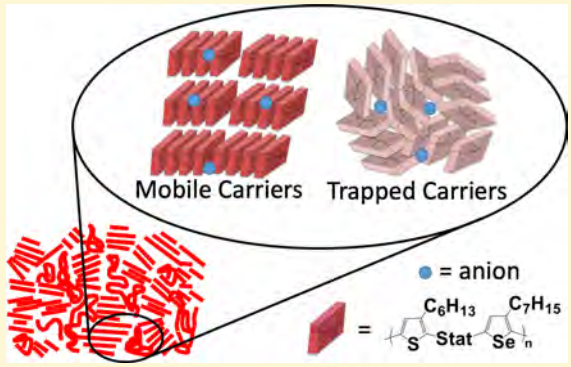

1. INTRODUCTION

Molecular doping has been shown to be a promising way to tune the electrical properties of semiconducting polymers for a variety of applications; for example, doped conjugated polymers show promise as the active material in organic thermoelectrics.[1] This is because when conjugated polymers are chemically doped with strong oxidizing agents such as 2,3,5,6-tetrafluoro-7,7,8,8-tetracyanoquinodimethane (F_4TCNQ; see Figure 1(f) for chemical structure)[2−4] or $FeCl_3$,[5] their intrinsically low electrical conductivities can be improved by orders of magnitude.[3] To achieve the highest possible conductivities, extremely high doping concentrations are usually required. Depending on the processing conditions, however, high doping levels can be difficult to achieve without disrupting the polymer film morphology.[6,7] This is because most conjugated polymers are soluble in weakly polar aromatic solvents, but when such polymers are heavily doped in solution and thus become electrically charged, they are generally no longer soluble, making it difficult to form good films by solution processing.

Received: June 22, 2018
Revised: December 1, 2018
Published: December 10, 2018

Downloaded via UNIV OF CALIFORNIA LOS ANGELES on January 8, 2019 at 23:29:57 (UTC).
See https://pubs.acs.org/sharingguidelines for options on how to legitimately share published articles.

© 2018 American Chemical Society

DOI: 10.1021/acs.chemmater.8b02648
Chem. Mater. 2019, 31, 73−82

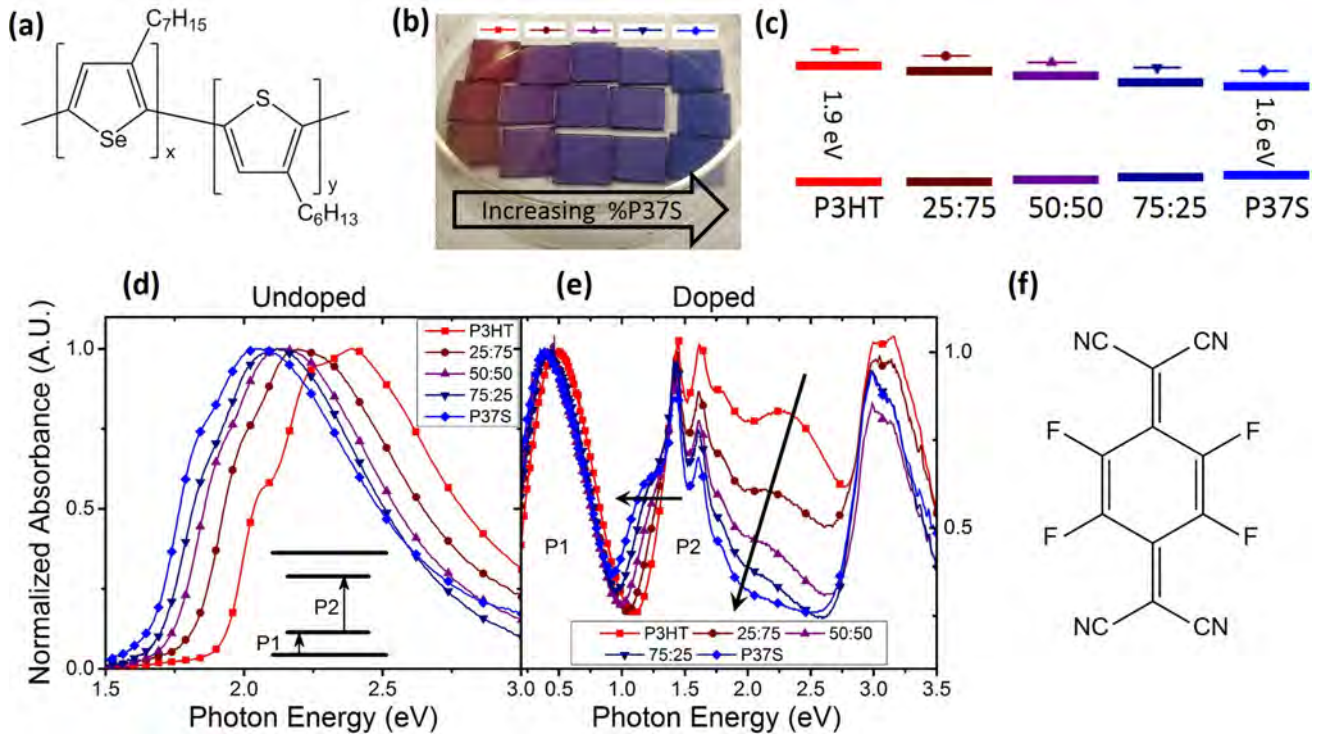

Figure 1. (a) Chemical structure of P37S-*stat*-P3HT copolymers. (b) Optical image of P37S-*stat*-P3HT films ranging in composition from 0 to 100% P37S in 25% increments, showing three films of each composition. (c) Cartoon schematic of the estimated change in valence and conduction band levels (consistent with the measured optical bandgap) of the copolymers as a function of P37S composition. (d) UV−visible absorbance of P37S-*stat*-P3HT copolymer films, normalized to the absorption maximum. The inset shows an energy level diagram indicating the allowed polaron transitions upon chemical doping. (e) UV−visible−NIR absorbance of P37S-*stat*-P3HT copolymer films that were doped by SqP with 1 mg/mL F_4TCNQ in DCM, normalized to the intensity of the P1 polaron absorption near 0.5 eV. (f) Chemical structure of F_4TCNQ. The arrows in panel e show the trends in doped-film absorption with increasing selenophene content.

There have been several recent approaches in the literature to overcome the difficulties with producing high-quality films of heavily doped conjugated polymers. One method has been to synthetically improve the solubility of the materials,[8,9] allowing for higher doping concentrations to be used without ultimately disturbing the doped film morphology.[7,10−12] Another method is based on doping by sequential processing (SqP), which has recently been shown to produce highly doped semiconducting polymer films without compromising film quality.[7,11] Doping by SqP works by first pre-casting a neutral polymer film and then infiltrating the dopant in a second casting step using a solvent that swells but does not dissolve the underlying film. Although it requires two processing steps, doping by SqP provides the advantage that the original neutral film morphology is largely preserved through the doping process. Thus, doping by SqP not only allows the fabrication of heavily doped films with outstanding morphology but also allows the crystallinity of the doped film to be controlled by choosing the conditions under which the original neutral film is cast.[13] For example, in previous work, we were able to use SqP to study how the optical and electrical properties of F_4TCNQ-doped films of poly(3-hexylthiophene-2,5-diyl) (P3HT) changed as the crystallinity of the P3HT was controllably varied.[13]

Although P3HT has been the workhorse conjugated polymer when it comes to studies of molecular doping, it is generally straightforward to rationally modify the chemical structure of conjugated polymers via synthesis to yield desired electrical or structural properties. One way to do this is to start with the traditional P3HT backbone, but to statistically replace some of the 3-hexylthiophene units with 3-heptylselenophene (37S), resulting in P37S-*stat*-P3HT copolymers with the structure indicated in Figure 1(a).[14,15] (We choose the heptyl side chain for the selenophene units instead of hexyl because the heptyl side chains both improve solubility and give a film morphology closer to that of P3HT;[15] see the Supporting Information for synthetic details.) The incorporation of the larger Se atom is known to increase the polymer crystallinity,[14,16,17] which is expected to be related to carrier mobility.[13] The addition of precise amounts of selenophene to the P3HT backbone also controllably shrinks the bandgap (Figures 1(b−d)) due to both lowering the conduction band and slightly raising the valence band relative to unmodified P3HT[16] (Figure 1(c)), both of which have significant implications for doping.

The purpose of this paper is to use a series of doped P37S-*stat*-P3HT copolymers to study the interplay of energy level offset and polymer crystallinity in determining the ease of doping and the resultant carrier mobility as both the energy level offset and crystallinity are incrementally tuned with polymer composition. We characterize the structure and crystallinity of the neutral and doped copolymer films using 2-D grazing incidence wide-angle X-ray scattering (GIWAXS) and differential scanning calorimetry (DSC) measurements. We then examine the swellability of the different statistical copolymer films using spectroscopic ellipsometry/porosimetry and find that both the density of mobile carriers produced by doping and the crystallinity of the polymer film after doping

DOI: 10.1021/acs.chemmater.8b02648
Chem. Mater. 2019, 31, 73−82

are directly influenced by the ability of the pre-doped film to swell during SqP.

We find that the doped film crystallinity has a pronounced effect on the conductivity and other optoelectrical properties. We use optical/NIR spectroscopy to show that the degree of polaron delocalization depends more on the film crystallinity than the band gap. We also use AC magnetic field Hall effect measurements to show that the carrier mobility, and thus the conductivity, is more influenced by the local structural environment than the energy level offset. Overall, the use of a tunable series of copolymers allows us to optimize carrier conductivity by balancing the trade-off between doped carrier concentration and carrier mobility.

2. CHARACTERIZING NEUTRAL AND DOPED P37S-*STAT*-P3HT COPOLYMERS

As described in more detail in the Supporting Information, we synthesized a series P37S-*stat*-P3HT copolymers with selenophene content ranging from 0 to 100% in 25% increments. Films of each of the copolymers, photos of which are shown in Figure 1(b), were prepared by dissolving the polymer powders in *o*-dichlorobenzene (ODCB) at a concentration of 1.5 mg/mL, while films of the P3HT and P37S homopolymers were prepared from solutions at a concentration of 2 mg/mL. Because heating was required to achieve full dissolution of the higher-Se-ratio copolymers, for consistency, we heated all of the polymer solutions to 100 °C prior to spin-coating at a rate of 1000 rpm for 60 s. Doped copolymer films were prepared via SqP by dissolving F_4TCNQ at a concentration of 1 mg/mL in dichloromethane (DCM) and spin-coating this solution on top of the pre-cast polymer films at 4000 rpm for 10 s. Successful employment of the SqP doping method requires a detailed understanding of both how the solvent and the dopant interact with each copolymer, which we describe in detail below.

2.1. Optical Absorption of SqP-Doped P37S-*stat*-P3HT Copolymers. After incorporation of the dopant into the polymer film has occurred, the molecular interaction of the dopant and the polymer is largely dependent on the energy level offset between the HOMO/valence band of the polymer and the LUMO of F_4TCNQ. As the selenophene ratio increases across the copolymer series, the optical bandgap changes from 1.9 eV for pure P3HT to 1.6 eV for pure P37S (see Figure 1(c)),[16] with the gap reduction mostly coming from a decrease of the copolymer LUMO/conduction band level. This shrinking of the bandgap is manifest as a redshift in the UV−visible absorption of the films, as seen in Figure 1(d), resulting in a noticeable color change across the copolymer series (as also shown in the photo of three films of each composition in Figure 1(b)).

We note that others have observed that the open circuit voltage (V_{OC}) of polymer-based photovoltaics containing a selenophene homopolymer is ∼0.1 eV lower than similar devices based on the thiophene analogues.[16] Because the V_{OC} of a bulk heterojunction photovoltaic can be used as a rough approximation of the energy level offset between the polymer donor HOMO level and the acceptor molecule LUMO level, and because the acceptor molecule used for both selenophene and thiophene analogues was the same, it is reasonable to assume that the difference in V_{OC} was purely due to a change in the polymer HOMO level. This indicates that the narrowing of the bandgap for the copolymer series from 100% P3HT to 100% P37S is a result of both the HOMO slightly raising[18] by ∼0.1 eV and the LUMO lowering[15,16,19] by ∼0.2 eV to account for the rest of the difference in bandgap. This implies that the HOMO levels of the copolymers are compositionally dependent, with more Se-heavy copolymer compositions having shallower HOMO levels. To verify this, we performed cyclic voltammetry (CV) measurements on the copolymer series; the details of which can be found in the Supporting Information. Within error, the CV measurements confirm that the HOMO levels of the copolymers slightly increase in energy with increasing selenophene content. This composition dependence of the HOMO level could affect the driving force for charge transfer from the polymer to the dopant.[3]

Figure 1(e) shows what happens to the optical properties when we take these same copolymer films and dope them by SqP with 1 mg/mL F_4TCNQ in DCM. The figure shows that the magnitude of the neutral exciton absorption peak decreases the most for the 100% P37S film relative to the rest of the series, which is summarized by the downward-pointing black arrow in Figure 1(e) and more quantitatively by the black crosses in Figure 2(b). This suggests that there is a higher level

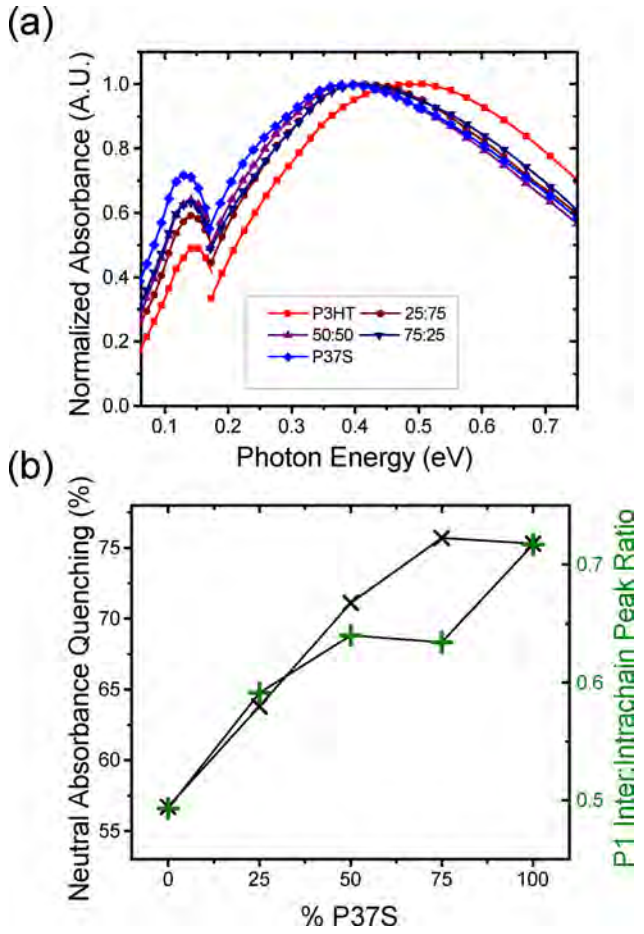

Figure 2. (a) Absorbance of the P1 polaron peak in P37S-*stat*-P3HT copolymer films doped by SqP with 1 mg/mL F_4TCNQ in DCM; the spectra are normalized by the height of the peak near ∼0.45 eV for ease of comparison. All of the spectra, including the IR active vibration peaks, were smoothed to allow for better visualization of relative peak locations and heights; the raw unsmoothed data are available in the Supporting Information. (b) Plots quantifying the depletion of the neutral absorbance intensity (black crosses) and the interchain to intrachain polaron peak ratio (green plus signs, from the data in panel a).

DOI: 10.1021/acs.chemmater.8b02648
Chem. Mater. 2019, 31, 73−82

of integer charge transfer with increasing selenophene content, consistent with the idea that increased selenophene content results in a larger energy level offset between the valence band of the copolymer and F_4TCNQ.

Quantifying the extent of doping from the loss of the neutral exciton peak is not straightforward, however, because the F_4TCNQ anion absorbs strongly with peaks at ~1.45 and ~1.65 eV, overlapping with the neutral absorption of the higher-selenophene content copolymers. Subtracting the anion absorption to uncover the loss of neutral copolymer absorption is also not readily achievable because the so-called P2 polaron peak, centered between ~1.2 and ~1.5 eV, also absorbs in this region. Moreover, the P2 absorption shifts with copolymer composition, as indicated by the horizontal arrow in Figure 1(e). In addition, we recently showed that for pure P3HT, the absorption cross-section of the polaron varies with the local polymer structural environment, and more importantly, that the number of mobile (as opposed to trapped) carriers created by doping is not a constant fraction of the total number of charged carriers created.[13] Thus, it is not possible with the information at hand to utilize absorption spectroscopy to quantify the number of mobile carriers produced upon doping of our copolymer series. A more detailed discussion on why absorption spectroscopy is not a reliable method for estimating the electrical properties of doped films is included in the Supporting Information.

Even though the absorption amplitudes are not useful for extracting quantitative information about mobile carriers, the position and shape of the spectra can tell us a lot about the local polaron environment.[13,20,21] Figure 2(a) shows a zoomed-in region of the "P1" polaron absorption constructed by stitching together UV−visible−NIR and FTIR spectra. The P1 polaron peak is split between an intrachain component in the 0.2−1.0 eV region and an interchain component in the region below 0.17 eV;[20,21] the spectra shown have been smoothed to allow for better comparison of the relative amplitudes of the two components. It is known that as the polaron becomes more delocalized and thus more mobile, the main intrachain peak redshifts and the relative amplitude of the lower-energy interchain absorption component increases.[13,20] Thus, the ratios of the intrachain and interchain components, which are presented as the green plus signs in Figure 2(b), are a reasonable measure of polaron delocalization and mobility.

The data in Figure 2(a) show that instead of the main polaron peak redshifting with increasing selenophene content, as expected based on the redshift of the bandgap,[22] the position of the main peak is nonmonotonic with composition, with a particularly large blue-shifted deviation for the 75:25 selenophene:thiophene material. This blue-shifted peak for the 75:25 composition is also accompanied by a lower inter/intrachain peak ratio (panel b)), suggesting that the polarons in this particular copolymer are less delocalized than would otherwise be expected given this material's position in the series. Moreover, the fact that the P2 transition (Figure 1(e)) shifts monotonically with the copolymer bandgap but the P1 transition does not reinforces the idea that the shape of the P1 polaron transition is extremely sensitive to its local structural environment. All of this indicates that when designing new materials for chemical doping, the energy levels are not the only important parameters to consider as other structural factors, considered in the next sections, can more drastically affect the functional properties of the doped material.

2.2. Crystallinity of Undoped P37S-*stat*-P3HT Copolymer Films. The advantage of studying a tunable series of thiophene-selenophene copolymers is that we can begin to decouple the effects of energy levels and crystallinity on the electrical properties of doped conjugated polymer films. We began our structural characterization by performing 2-D GIWAXS measurements on the undoped copolymers to quantify the relative crystallinity across the series. Figure 3(a) shows the radially integrated results for the undoped copolymers, with Table 1 reporting the integrated area and the *d*-spacing of the lamellar (100) peak, which represents the distance between polymer backbones in the direction along the polymer side chains. In- and out-of-plane integrations, which

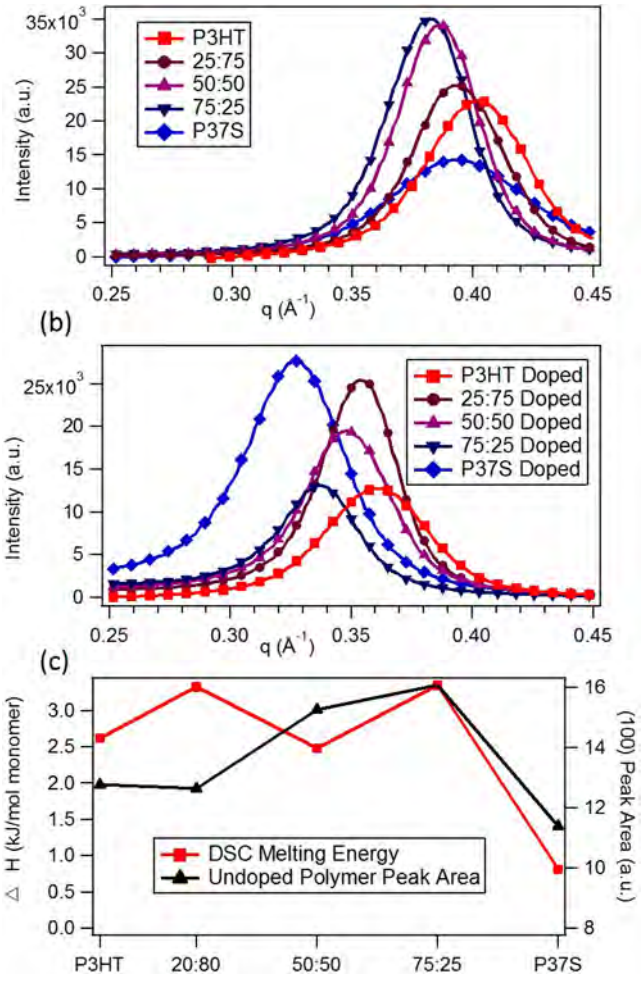

Figure 3. Radially integrated GIWAXS data for (a) the undoped copolymers and (b) the same polymer films after SqP doping with 1 mg/mL F_4TCNQ in DCM. The (100) peak of the undoped films shifts monotonically to larger *d*-spacing as the selenophene content is increased, as expected for the larger Se atom and longer side chains of the P37S monomer compared to P3HT, except for 100% P37S, as discussed in the text. The (100) peak of the doped films shifts to even larger *d*-spacing after F_4TCNQ has been incorporated. The peak positions and areas are summarized in Table 1; see the text for details. (c) DSC melting enthalpy (normalized per monomer unit) and integrated (100) peak area from GIWAXS and DSC as a function of increasing selenophene content. The good correlation indicates that GIWAXS does provide a good measure of relative crystallinity in each sample.

DOI: 10.1021/acs.chemmater.8b02648
Chem. Mater. 2019, 31, 73−82

Table 1. Relative Crystallinities, Based on the Radially-Integrated (100) Peak Area, and *d*-Spacings in Å, for both Pure and Doped Selenophene:Thiophene Copolymer Films, Along with the Shift in *d*-Spacing after Doping[a]

	100% P3HT	25:75	50:50	75:25	100% P37S
undoped (100) *d*-spacing (Å)	15.65	15.96	16.30	16.48	N/A
doped (100) *d*-spacing (Å)	17.43	17.80	18.06	18.74	19.30
shift in *d*-spacing (Å)	1.78	1.84	1.76	2.26	N/A
undoped (100) peak area	1276	1263	1525	1607	N/A
doped (100) peak area	716	1067	953	613	1592
ratio of doped/undoped	0.56	0.84	0.62	0.38	N/A

[a]The values for undoped 100% P37S are not included because this material has a different crystal structure (Type-II polymorph).

provide information on the crystalline domain orientation in each material, are given in the Supporting Information.

The GIWAXS data in Figure 3(a) show a clear trend of the (100) peak position shifting to smaller q (larger d-spacing), and the peak intensity increasing as the selenophene content is increased. The general trend of increasing d-spacing with increasing selenophene content makes sense given the fact that the selenophene units have heptyl side chains, while the thiophene monomers have slightly shorter hexyl side chains. We also examined the π-stacking (010) peak across the copolymer series and found similar trends as seen for the (100) peak. Details are given in the Supporting Information.

The exception to this trend is the (100) peak of the 100% P37S film, which shows a smaller lamellar spacing as well as significantly decreased intensity and broadening compared to the rest of the series. The fact that the 100% P37S film does not follow the trend is because pure P37S does not have the same crystal structure as the rest of the samples in the series. Instead of the more common Type-I polymorph, the pure P37S material exists as a Type-II polymorph, where the heptyl side chains are more interdigitated, explaining the smaller lamellar d-spacing in this sample.[17,23]

The increased d-spacing along the lamellar direction with greater selenophene content has important implications for the properties of the copolymer materials after doping. This is because when dopants such as F_4TCNQ reside in the crystalline regions of the film, they do so in the lamellar regions between the side chains.[12,13,24] The fact that the higher-selenophene content materials have more space along the side-chain direction potentially allows for the dopant anions to reside farther from the polymer backbones where the polarons are located, which would reduce the Coulomb interaction between them. Thus, the increased lamellar spacing could potentially help allow for reduced polaron localization.[13]

The trend in the radially integrated (100) peak intensities seen in Figure 3(a) reflect, in part, the relative crystallinities of the different copolymers. Unfortunately, conclusions about relative crystallinity are complicated by the fact that the different copolymers have different fractions of heavy selenophene atoms, which can affect both the structure factor and overall X-ray scattering power of each sample in the series. Taken at face value, the peak intensity increase with increasing selenophene content indicates increasing crystallinity, but some or all of this increased peak intensity could be due to increasing scattering contrast or a change in structure factor.

To better understand how the integrated (100) peak areas are related to relative copolymer crystallinity, we performed a series of DSC measurements on the as-synthesized copolymer powders to measure the enthalpies of melting (details in the Supporting Information); we could not perform the measurements directly on our spin-cast films due to the small amount of material present. Although the crystallinity of the powders may be different than that of spin-cast films, we do expect the enthalpy of melting for crystalline materials to be relatively constant across this series of copolymers, so any change in melting enthalpy can be associated with changes in the relative crystalline fraction of the materials.

The DSC-determined melting enthalpies, normalized per mole of monomer unit, are plotted as a function of selenophene content alongside the integrated (100) peak areas of the undoped samples in Figure 3(c). We chose the first melt enthalpy for this plot as we felt that this provided the best comparison to the properties of our solution-cast films, but we observed almost identical trends across the copolymer series for the melting and freezing enthalpies in both the first and second cycles. The general agreement between the DSC- and GIWAXS-derived data seen in Figure 3(c) suggests that although variations in structure factors and scattering power may influence the absolute X-ray scattering between different samples, the general trend of increasing crystallinity with increasing selenophene content observed by GIWAXS is correct.

Table 1 summarizes the results of Figure 3(a), of which the most important message is that the relative copolymer crystallinity does not scale monotonically with selenophene content. Instead, the undoped 75:25 selenophene:thiophene material is the most crystalline of the series, a fact that will become important when we consider how the SqP doping process alters the film crystallinity, as discussed in the next section.

2.3. Crystallinity of P37S-*stat*-P3HT Copolymer Films after Doping with F_4TCNQ by SqP. With the relative crystallinities of the undoped copolymer series characterized, we turn next to understanding the film structure after doping via SqP with 1 mg/mL F_4TCNQ in DCM. Figure 3(b) and Table 1 summarize the radially integrated GIWAXS data for the doped copolymers. The data show that the d-spacing of the (100) peak shifts to larger distances after F_4TCNQ has been introduced, as has been seen previously for other conjugated polymers.[2,7,13] Of particular note is that the (100) peak for doped 100% P37S shows the largest d-spacing, whereas this material had one of the smaller d-spacings of the undoped materials. We saw above that the undoped 100% P37S has a crystal structure (Type-II polymorph) different than that of the other copolymers, one with an inherently smaller lamellar d-spacing due to chain interdigitation. We also know that F_4TCNQ prefers to reside in the lamellar regions of P3HT crystallites,[12,13] leading us to believe that the incorporation of F_4TCNQ into the lamellar regions of the P37S crystallites is incompatible with this side-chain interdigitation. Thus, the doping process effectively converts the Type-II polymorph of 100% P37S to the more commonly observed Type-I polymorph, bringing the doped P37S material in line with the rest of the copolymers in the series.

Figure 3(b) also shows that the relative scattering intensities of the doped copolymers behave rather differently than those of the undoped films. Because of the scattering differences for polymers with different Se content, it is not straightforward to

DOI: 10.1021/acs.chemmater.8b02648
Chem. Mater. 2019, 31, 73−82

map these intensity differences onto changes in crystallinity. Thus, to best quantify changes in crystallinity after doping with F_4TCNQ, we calculated the ratios of the radially integrated (100) peak area before and after SqP doping (Figure 5 and Table 1). Because the Se/S ratio does not change before and after SqP doping, the before-to-after doping (100) peak area ratio should provide a good measure of the changes in crystallinity caused by doping. For P3HT, we note that recent work has argued that doping with F_4TCNQ causes changes in film morphology, including an increase in the average conjugation length of the amorphous chains outside the polymer crystallites.[25]

For our copolymers, we see that the change in overall crystallinity of the films as a result of the solution sequential doping process varies depending on the composition. The total crystallinity decreases significantly for the doped 100% P3HT film relative to the undoped film. This decrease in overall crystallinity is partly reversed for the 25:75 Se:S sample but then decreases slightly in the 50:50 material and significantly for the 75:25 Se:S sample. Note that the change in the 100% P37S upon doping cannot properly be compared to the other polymers in the series due to the fact that it undergoes a change in crystal structure upon doping, as mentioned above. The GIWAXS data for the $\pi-\pi$ stacking peak for the doped copolymer films show similar trends as for the lamellar stacking peak (see Supporting Information).

The changes in crystallinity we see upon doping can be explained by the idea that the dopant either disrupts or enhances some of the coherence in polymer chain packing as it sits in the lamellar regions of the crystallites. The solvent used during the sequential doping step swells the film, allowing some reorganization of the film morphology. Normally, as the solvent dries, the film would return to its pre-swollen state. However, by introduction of dopant molecules into the swollen polymer matrix, a new morphology can be created after the solvent evaporates. This is what allows the dopant to either disrupt some of the crystallinity within the crystalline domains or induce ordering in previously amorphous or poorly crystalline regions, depending on the interaction between the dopant and the polymer.

We note that the ability of the dopant to interact with and rearrange the film morphology is also dependent on the ability of the solvent to swell the polymer film, and that swelling ability generally decreases with increasing polymer crystallinity. This emphasizes the importance of the role the solvent plays for doping via SqP, as discussed in the next Section 2.4.

2.4. Quantifying the Solvent:Polymer Interaction for P37S-*stat*-P3HT Copolymers. Because the interaction between the solvent and the polymer is critical to being able to manipulate the morphology through the addition of dopant molecules, in this section we quantify the copolymer:solvent interaction to better understand the structural changes that take place as a result of the SqP doping process. In general, the swellability of a polymer film depends inversely on its crystallinity,[13,26] which varies across our copolymer series. We thus performed a series of swelling measurements by exposing the copolymer films to saturated DCM vapor, which mimics the exposure of the films to the DCM solvent we use in the SqP doping process. We then quantify the extent to which the films swell as they interact with the DCM vapor using spectroscopy ellipsometry (see the Supporting Information for experimental details and fits).

Figure 4 shows the swellability of the undoped copolymer films (bars). The data show that the swellability does not depend linearly or even monotonically on the copolymer composition. The undoped 75:25 selenophene:thiophene copolymer shows the least swellability, which is perhaps not surprising as this material is the most crystalline of the series.[13,26] The higher swellability of the other copolymers relative to 100% P3HT can be explained by the fact that the larger, more polarizable Se atoms provide for increased interactions with DCM relative to the smaller, less polarizable S atoms.

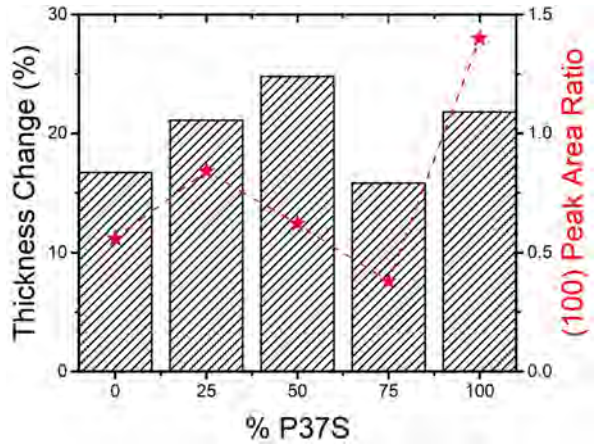

Figure 4. Percent change in film thickness due to swelling caused by exposure to DCM vapors as measured by ellipsometry (black bars) for the P37S-*stat*-P3HT copolymer series. Also plotted is the change in relative crystallinity as quantified by the ratio of the SqP doped film (100) peak area to the undoped film (100) peak area for each P37S-*stat*-P3HT copolymer in the series (orange stars).

Figure 4 also compares the copolymer swellability with the change in crystallinity of the films upon doping, as quantified by the ratio of the doped-to-undoped integrated (100) peak areas (orange stars); the trends of these two measures are in good general agreement. This correlation between swellability and change in crystallinity suggests that SqP for fullerene infiltration and SqP for doping can affect film structure in different ways. When SqP is used for fullerene infiltration, fullerene is deposited only into the amorphous regions of the film and the crystalline structure of the pre-cast polymer film is preserved. The SqP doping process, in contrast, requires dopant infiltration into crystalline domains, so materials where the crystalline domains are not effectively swollen are also not effectively doped. This direct correlation between swelling and crystallinity after doping has not been previously observed or investigated, although dopant-induced increases in crystallinity have been reported.[24,25]

Clearly, optimization of the solvent:polymer interaction is not only possible but critical to the success of SqP doping, as different solvents produce different degrees of swelling, which in turn alters the ability of dopants to induce changes in the film morphology. We will investigate such optimization in future work.

2.5. Electrical Characterization of SqP-Doped P37S-*stat*-P3HT. Given the nonmonotonic trend of swellability and crystallinity change upon doping across the copolymer series, the next logical question to address is how these structural trends correlate with the functional electrical properties of the

DOI: 10.1021/acs.chemmater.8b02648
Chem. Mater. 2019, 31, 73−82

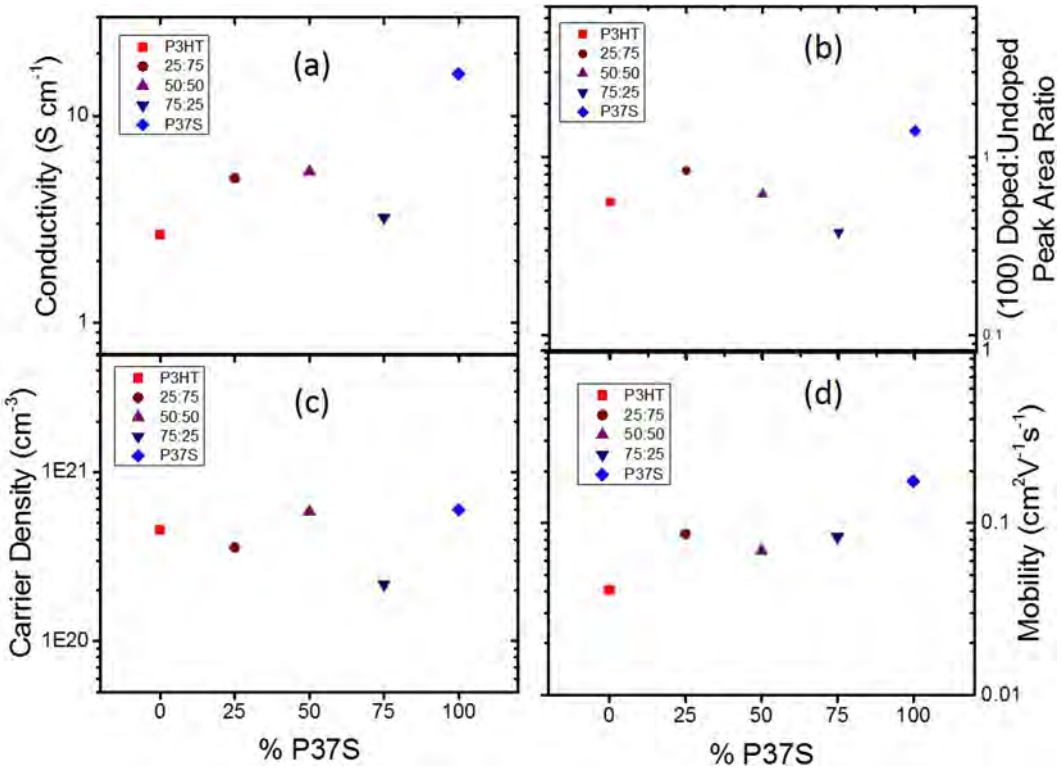

Figure 5. Semilogarithmic plots of (a) electrical conductivity, (b) doped:undoped (100) peak area ratio, (c) carrier density, extracted from AC Hall effect measurements, and (d) carrier mobility, calculated from the ratio of the conductivity and carrier density, all as a function of selenophene content across the copolymer series. All of the electrical measurements were for films doped by SqP with 1 mg/mL F_4TCNQ in DCM.

doped copolymers. We performed electrical conductivity measurements using four-point-probe measurements in both collinear and Van der Pauw geometries; details are given in the Supporting Information. The results, summarized in Figure 5(a), show that the conductivity increases for the 25:75 and 50:50 selenophene:thiophene copolymers but then drops significantly for the 75:25 selenophene:thiophene copolymer. Notably, the conductivity follows a similar trend to the change in crystallinity upon doping, as quantified by doped:undoped (100) peak area ratio (Figure 5(b)). Moreover, for 100% P37S, the conductivity can exceed 20 S/cm, providing an order of magnitude increase over the conductivity of 100% P3HT simply by substituting selenophene for thiophene.

To determine whether the improvement in conductivity results from the higher valence band of P37S, the larger swellability of the selenophene polymer in DCM, the increased relative crystallinity of the selenophene polymer after doping, or some combination of all of these, we employed AC magnetic field Hall effect measurements[7,13,27−30] to determine how the conductivity of each copolymer results from the product of carrier mobility and carrier concentration. AC Hall measurements are different from traditional DC Hall effect measurements in that the magnetic field is alternated in a time-dependent manner such that the Hall voltage becomes similarly time dependent. This allows one to lock in on the Hall voltage and disregard the intrinsic offset voltage which is not time dependent and is often large enough to obscure the Hall voltage in low mobility materials such as semiconducting polymers.

The results of the AC Hall measurements yield Hall charge carrier densities (n_H, shown for the copolymer series in Figure 5(c)), which are connected to the carrier mobility (μ_H, Figure 5(d)) and conductivity (σ, Figure 5(a)) by $\sigma = n_H q \mu_H$, where q is the fundamental charge. We note that in low-mobility materials such as doped conjugated polymers, the carrier density extracted from AC Hall effect measurements can be subject to error because carriers that move by hopping can screen the magnetic field of neighboring carriers.[30,31] Based on our previous work studying P3HT[13] and the results discussed below, however, we believe that the copolymers studied here all share a similar hopping-dominated transport mechanism, and thus even if the absolute carrier densities are subject to some error, the relative comparison across the copolymer series should be fairly accurate.

Figure 5(c) shows the mobile carrier density extracted from the AC Hall effect measurements made on the SqP-doped P37S-*stat*-P3HT series; details of how the measurements were made are given in the Supporting Information. The data make clear that the mobile carrier density remains nearly constant (or perhaps slightly increases) with increasing selenophene content, with the exception of the 75:25 selenophene:thiophene copolymer, which has a significantly lower mobile carrier density (note that Figure 5(c) has the carrier density plotted on a logarithmic scale). The slight increase across the series would fit well with the idea that there is increased driving force for doping as the energy level offset increases with increasing selenophene content (and also fits with the increase in quenching of the neutral polymer absorbance seen in Figure 2(b)), although this is a relatively minor effect.

The drop in mobile carrier density for the 75:25 selenophene:thiophene copolymer correlates with the significant decrease in crystallinity upon doping in this material, as seen in Figure 5(b). The high crystallinity likely prevents the F_4TCNQ dopant from effectively incorporating into crystalline

DOI: 10.1021/acs.chemmater.8b02648
Chem. Mater. 2019, 31, 73−82

parts of this copolymer during the SqP doping process. Instead, reaction with F_4TCNQ drives a transition to an amorphous geometry where the F_4TCNQ anion can find space in the polymer network. The mobility data can then be explained by the hypothesis that the majority of mobile carriers are formed by doping the crystalline regions of the film, where the dopant anions are forced to lie farther away from the polarons on the polymer backbone, thus reducing Coulomb trapping and increasing polaron mobility. Dopant anions in the amorphous regions of the film, in contrast, can sit in closer Coulomb contact to their corresponding polarons. These Coulombically bound carriers would appear optically but would not contribute to the Hall voltage because they are effectively trapped. This idea is consistent with the fact that the 72:25 selenophene:thiophene sample shows a P1 absorption that is blue-shifted and has a low interchain to intrachain absorption ratio, both of which are signatures of a higher fraction of less mobile or trapped carriers.

We also might expect the depletion of the neutral absorption peak across the series after doping to track with the carrier concentration, but a comparison of Figure 5(c) to Figure 2(b) shows that this is not the case, verifying our argument above that UV−visible absorption is not a good method for determining the mobile carrier concentration in doped conjugated polymer films: the facts that both trapped and mobile carriers contribute to the absorption and that the degree of mobility/trapping changes the absorption position, shape and cross-section make it effectively impossible to correlate optical properties with electrical properties that depend only on mobile carriers.

Figure 5(d) shows the carrier mobility extracted from the Hall effect measurements. The mobility shows a very different trend from the carrier concentration, with no dramatic dip for the 75:25 composition and instead a gradual increase in mobility with increasing selenophene content. This general increase in carrier mobility with selenophene content is largely responsible for the increased conductivity across the series, as the carrier density remains relatively constant from 100% P3HT to 100% P37S, with the exception of the highly crystalline 75:25 material.

Overall, by far the strongest correlation of the conductivity to film structure is the fractional change in crystallinity of the doped material. This suggests that if the dopant cannot fit well into the polymer lattice in an ordered manner, there will be an energetic penalty for incorporation. In this situation, less dopant will incorporate in positions that produce mobile carriers. Although trapped carriers can be produced (and observed by optical absorption), these trapped carriers do not contribute to the overall conductivity, as discussed above.

We reached a similar conclusion concerning polymer structure and carrier mobility in our previous work studying doped P3HT films with different controlled amounts of crystallinity.[13] This work, however, highlights the fact that the crystallinity of the undoped film is not the key parameter in determining carrier mobility, but rather the crystallinity of the film after doping. The crystallinity of films doped by SqP, in turn, depends on both their original crystallinity, their swellability, and the ability of the polymer lattice to accommodate dopant molecules within the crystal structure. Thus, when designing new conjugated polymers for applications with chemical doping, it is important to consider not only the crystallinity of the neutral polymer but the ability of the polymer to swell during SqP and then crystallize when doped. The 100% P37S polymer does both of these well, allowing us to readily achieve electrical conductivities exceeding 20 S/cm by SqP doping with only 1 mg/mL F_4TCNQ.

3. SUMMARY AND CONCLUSIONS

We showed that the bandgap, valence band position, crystallinity, and swellability of undoped P3HT, as well as the change in crystallinity after doping by SqP with F_4TCNQ, can be controllably tuned by synthetic statistical substitution with selenophene units, although not all the changes are monotonic with fractional selenophene composition. The bandgap decreases monotonically, and the valence band slightly increases monotonically as the copolymer composition is tuned from 100% P3HT to 100% P37S. The change in valence band position provides for an increase in carrier concentration upon doping as the fraction of selenophene increases, but not all the carriers created are mobile. Instead, it is the way increasing selenophene content changes polymer structure and crystallinity that provides the best correlation with the optical and electrical properties of the materials after doping. The key relation is that electrical conductivity depends on the ability of the dopant to restructure the polymer, which in turn depends on the polymer's ability to swell and its ability to accommodate the dopant within its lattice.

The 75:25 selenophene:thiophene copolymer is the most crystalline in its undoped form, making it the least swellable material in our copolymer series. This lack of swellability also gives this material the lowest mobile carrier concentration when doped, despite having a relatively high valence band and good energy level offset from F_4TCNQ and a strong depletion of the neutral exciton absorption. Correlated with the fact that this copolymer has a lower mobile carrier concentration is that it shows the largest decrease in crystallinity upon doping, suggesting that this material simply cannot effectively accommodate F_4TCNQ molecules within its lattice. The free carrier concentration measured by the AC Hall effect does not match with the depletion of the neutral absorption peak, indicating that there are either large changes in absorption cross-section and/or significant fractions of trapped carriers. The hypothesis that many carriers are trapped is supported by the relatively blue-shifted polaron absorption of this member of the series.

Across the copolymer series, we see that it is the crystallinity of the doped state that ultimately determines the mobile carrier concentration. This suggests that the majority of dopants in amorphous regions of the polymer produced trapped carriers, and that mobile carriers are only produced when they are spatially separated from their counterions because of the limited number of places that the F_4TCNQ anions can reside within the crystalline lattice. This idea is corroborated by optical spectroscopy, which shows excellent correlation between the position and shape of the polaron P1 transition, the crystallinity of the doped film, and the mobile carrier mobility. The polaron P2 transition, however, does not appear to be strongly affected by the local environment and instead scales simply with the bandgap of the polymer. The P1 and P2 absorption amplitudes do not correlate with the number of mobile carriers in the films, preventing optical spectroscopy from being used to quantify the mobile carrier concentration.

In the end, achieving the highest mobilities requires not only a good degree of intrinsic crystallinity but also swellability, which determines how well the dopant can infiltrate the material, and the general ability of the polymer lattice to

DOI: 10.1021/acs.chemmater.8b02648
Chem. Mater. 2019, 31, 73−82

accommodate dopants within their crystalline domains. For our copolymer series, these requirements were best met by the 100% P37S material, giving it the highest carrier concentration and highest carrier mobility, leading to electrical conductivities that exceed 20 S/cm at higher doping levels. Overall, the electrical, structural, and optical measurements across the P3HT-*stat*-P37S copolymer series all corroborate the crystallinity of the doped state being the dominant factor that influences the properties of highly doped semiconducting polymer films.

■ ASSOCIATED CONTENT

Supporting Information

The Supporting Information is available free of charge on the ACS Publications website at DOI: 10.1021/acs.chemmater.8b02648.

Details on the synthesis and characterization of the copolymers and spectroscopy, GIWAXS, DSC, cyclic voltammetry, spectroscopic ellipsometry, and AC Hall measurements, including raw data and methods of analysis (PDF)

■ AUTHOR INFORMATION

Corresponding Authors

*E-mail: tolbert@chem.ucla.edu.
*E-mail: schwartz@chem.ucla.edu.

ORCID

Dwight S. Seferos: 0000-0001-8742-8058
Sarah H. Tolbert: 0000-0001-9969-1582
Benjamin J. Schwartz: 0000-0003-3257-9152

Notes

The authors declare no competing financial interest.

■ ACKNOWLEDGMENTS

This work was supported by the National Science Foundation under Grants CBET-1510353 and CHE-1608957. The X-ray diffraction studies presented in this manuscript were carried out at the Stanford Synchrotron Radiation Lightsource. Use of the Stanford Synchrotron Radiation Lightsource, SLAC National Accelerator Laboratory, is supported by the U.S. Department of Energy, Office of Science, Office of Basic Energy Sciences, under Contract DEAC02-76SF00515. This work was supported by the NSERC of Canada.

■ REFERENCES

(1) Russ, B.; Glaudell, A.; Urban, J. J.; Chabinyc, M. L.; Segalman, R. A. Organic thermoelectric materials for energy harvesting and temperature control. *Nat. Rev. Mater.* **2016**, *1*, 16050.

(2) Duong, D. T.; Wang, C.; Antono, E.; Toney, M. F.; Salleo, A. The chemical and structural origin of efficient p-type doping in P3HT. *Org. Electron.* **2013**, *14*, 1330−1336.

(3) Yim, K.-H.; Whiting, G. L.; Murphy, C. E.; Halls, J. J. M.; Burroughes, J. H.; Friend, R. H.; Kim, J.-S. Controlling Electrical Properties of Conjugated Polymers via a Solution-Based p-Type Doping. *Adv. Mater.* **2008**, *20*, 3319−3324.

(4) Pingel, P.; Neher, D. Comprehensive picture of p-type doping of P3HT with the molecular acceptor F4TCNQ. *Phys. Rev. B: Condens. Matter Mater. Phys.* **2013**, *87*, 115209.

(5) Yamamoto, J.; Furukawa, Y. Electronic and Vibrational Spectra of Positive Polarons and Bipolarons in Regioregular Poly(3-hexylthiophene) Doped with Ferric Chloride. *J. Phys. Chem. B* **2015**, *119*, 4788−4794.

(6) Deschler, F.; Riedel, D.; Deák, A.; Ecker, B.; von Hauff, E.; Da Como, E. Imaging of morphological changes and phase segregation in doped polymeric semiconductors. *Synth. Met.* **2015**, *199*, 381−387.

(7) Scholes, D. T.; Hawks, S. A.; Yee, P. Y.; Wu, H.; Lindemuth, J. R.; Tolbert, S. H.; Schwartz, B. J. Overcoming Film Quality Issues for Conjugated Polymers Doped with F4 TCNQ by Solution Sequential Processing: Hall Effect, Structural, and Optical Measurements. *J. Phys. Chem. Lett.* **2015**, *6*, 4786−4793.

(8) Li, J.; Zhang, G.; Holm, D. M.; Jacobs, I. E.; Yin, B.; Stroeve, P.; Mascal, M.; Moulé, A. J. Introducing Solubility Control for Improved Organic P-Type Dopants. *Chem. Mater.* **2015**, *27*, 5765−5774.

(9) Kroon, R.; Kiefer, D.; Stegerer, D.; Yu, L.; Sommer, M.; Müller, C. Polar Side Chains Enhance Processability, Electrical Conductivity, and Thermal Stability of a Molecularly p-Doped Polythiophene. *Adv. Mater.* **2017**, *29*, 1700930.

(10) Müller, L.; Nanova, D.; Glaser, T.; Beck, S.; Pucci, A.; Kast, A. K.; Schröder, R. R.; Mankel, E.; Pingel, P.; Neher, D.; Kowalsky, W.; Lovrincic, R. Charge-Transfer-Solvent Interaction Predefines Doping Efficiency in p-Doped P3HT Films. *Chem. Mater.* **2016**, *28*, 4432−4439.

(11) Jacobs, I. E.; Aasen, E. W.; Oliveira, J. L.; Fonseca, T. N.; Roehling, J. D.; Li, J.; Zhang, G.; Augustine, M. P.; Mascal, M.; Moulé, A. J. Comparison of solution-mixed and sequentially processed P3HT:F4TCNQ films: effect of doping-induced aggregation on film morphology. *J. Mater. Chem. C* **2016**, *4*, 3454−3466.

(12) Hamidi-Sakr, A.; Biniek, L.; Bantignies, J.-L.; Maurin, D.; Herrmann, L.; Leclerc, N.; Lévêque, P.; Vijayakumar, V.; Zimmermann, N.; Brinkmann, M. A Versatile Method to Fabricate Highly In-Plane Aligned Conducting Polymer Films with Anisotropic Charge Transport and Thermoelectric Properties: The Key Role of Alkyl Side Chain Layers on the Doping Mechanism. *Adv. Funct. Mater.* **2017**, *27*, 1700173.

(13) Scholes, D. T.; Yee, P. Y.; Lindemuth, J. R.; Kang, H.; Onorato, J.; Ghosh, R.; Luscombe, C. K.; Spano, F. C.; Tolbert, S. H.; Schwartz, B. J. The Effects of Crystallinity on Charge Transport and the Structure of Sequentially Processed F 4 TCNQ-Doped Conjugated Polymer Films. *Adv. Funct. Mater.* **2017**, *27*, 1702654.

(14) Hollinger, J.; Jahnke, A. A.; Coombs, N.; Seferos, D. S. Controlling Phase Separation and Optical Properties in Conjugated Polymers through Selenophene-Thiophene Copolymerization. *J. Am. Chem. Soc.* **2010**, *132*, 8546−8547.

(15) Hollinger, J.; Sun, J.; Gao, D.; Karl, D.; Seferos, D. S. Statistical Conjugated Polymers Comprising Optoelectronically Distinct Units. *Macromol. Rapid Commun.* **2013**, *34*, 437−441.

(16) Heeney, M.; Zhang, W.; Crouch, D. J.; Chabinyc, M. L.; Gordeyev, S.; Hamilton, R.; Higgins, S. J.; McCulloch, I.; Skabara, P. J.; Sparrowe, D.; Tierney, S. Regioregular poly(3-hexyl)selenophene: a low band gap organic hole transporting polymer. *Chem. Commun.* **2007**, 5061.

(17) Li, L.; Hollinger, J.; Jahnke, A. a.; Petrov, S.; Seferos, D. S. Polyselenophenes with distinct crystallization properties. *Chem. Sci.* **2011**, *2*, 2306.

(18) Manion, J. G.; Ye, S.; Proppe, A. H.; Laramée, A. W.; McKeown, G. R.; Kynaston, E. L.; Kelley, S. O.; Sargent, E. H.; Seferos, D. S. Examining Structure−Property−Function Relationships in Thiophene, Selenophene, and Tellurophene Homopolymers. *ACS Applied Energy Materials* **2018**, *1*, 5033.

(19) Yan, H.; Hollinger, J.; Bridges, C. R.; McKeown, G. R.; Al-Faouri, T.; Seferos, D. S. Doping Poly(3-hexylthiophene) Nanowires with Selenophene Increases the Performance of Polymer-Nanowire Solar Cells. *Chem. Mater.* **2014**, *26*, 4605−4611.

(20) Ghosh, R.; Pochas, C. M.; Spano, F. C. Polaron Delocalization in Conjugated Polymer Films. *J. Phys. Chem. C* **2016**, *120*, 11394−11406.

(21) Pochas, C. M.; Spano, F. C. New insights on the nature of two-dimensional polarons in semiconducting polymers: Infrared absorption in poly(3-hexylthiophene). *J. Chem. Phys.* **2014**, *140*, 244902.

(22) Wohlgenannt, M.; Jiang, X. M.; Vardeny, Z. V. Confined and delocalized polarons in π-conjugated oligomers and polymers: A study

DOI: 10.1021/acs.chemmater.8b02648
Chem. Mater. 2019, 31, 73−82

of the effective conjugation length. *Phys. Rev. B: Condens. Matter Mater. Phys.* **2004**, *69*, 241204.
(23) Prosa, T. J.; Winokur, M. J.; McCullough, R. D. Evidence of a novel side chain structure in regioregular poly(3-alkylthiophenes). *Macromolecules* **1996**, *29*, 3654−3656.
(24) Kang, K.; Watanabe, S.; Broch, K.; Sepe, A.; Brown, A.; Nasrallah, I.; Nikolka, M.; Fei, Z.; Heeney, M.; Matsumoto, D.; Marumoto, K.; Tanaka, H.; Kuroda, S.-i.; Sirringhaus, H. 2D coherent charge transport in highly ordered conducting polymers doped by solid state diffusion. *Nat. Mater.* **2016**, *15*, 896−902.
(25) Chew, A. R.; Ghosh, R.; Shang, Z.; Spano, F. C.; Salleo, A. Sequential Doping Reveals the Importance of Amorphous Chain Rigidity in Charge Transport of Semi-Crystalline Polymers. *J. Phys. Chem. Lett.* **2017**, *8*, 4974−4980.
(26) Aguirre, J. C.; Hawks, S. A.; Ferreira, A. S.; Yee, P.; Subramaniyan, S.; Jenekhe, S. A.; Tolbert, S. H.; Schwartz, B. J. Sequential Processing for Organic Photovoltaics: Design Rules for Morphology Control by Tailored Semi-Orthogonal Solvent Blends. *Adv. Energy Mater.* **2015**, *5*, 1402020.
(27) Lindemuth, J.; Mizuta, S.-I. Hall measurements on low-mobility materials and high resistivity materials. *Proc. SPIE* **2011**, *8110*, 81100I.
(28) Lindemuth, J. Variable temperature Hall measurements on low-mobility materials. *Proc. SPIE* **2012**, *8470*, 84700G.
(29) Chen, Y.; Yi, H. T.; Podzorov, V. High-Resolution ac Measurements of the Hall Effect in Organic Field-Effect Transistors. *Phys. Rev. Appl.* **2016**, *5*, 034008.
(30) Fujimoto, R.; Watanabe, S.; Yamashita, Y.; Tsurumi, J.; Matsui, H.; Kushida, T.; Mitsui, C.; Yi, H. T.; Podzorov, V.; Takeya, J. Control of molecular doping in conjugated polymers by thermal annealing. *Org. Electron.* **2017**, *47*, 139−146.
(31) Yi, H. T.; Gartstein, Y. N.; Podzorov, V. Charge carrier coherence and Hall effect in organic semiconductors. *Sci. Rep.* **2016**, *6*, 23650.

DOI: 10.1021/acs.chemmater.8b02648
Chem. Mater. 2019, 31, 73−82